

## Deviations from NLO QCD evolution in inclusive HERA data

Fabrizio Caola, Stefano Forte and Juan Rojo

*Dipartimento di Fisica, Università di Milano and INFN, Sezione di Milano,  
Via Celoria 16, I-20133 Milano, Italy*

### Abstract:

We search for deviations from next-to-leading order QCD evolution in HERA structure function data. We compare to data predictions for structure functions in the small  $x$  region, obtained by evolving backwards to low  $Q^2$  the results of a parton fit performed in the large  $Q^2$  region, where fixed-order perturbative QCD is certainly reliable. We find evidence for deviations which are qualitatively consistent with the behaviour predicted by small  $x$  perturbative resummation, and possibly also by nonlinear evolution effects, but incompatible with next-to-next-to-leading order corrections.

There are several reasons to expect that fixed-order next-to-leading perturbative QCD evolution (NLO DGLAP [1] evolution, henceforth) might fail to provide an adequate description of experimental data for small enough values of Bjorken  $x$  and of  $Q^2$ . These include the presence of higher order corrections, which are large at small  $x$  [2, 3], the possible impact of all-order resummation of large small  $x$  logs [4] or non linear phenomena which are expected to restore unitarity in the high energy limit [5]. On the other hand, available QCD analysis based on NLO DGLAP [3, 6, 7] are known to provide an excellent description of HERA data, which implies that such deviations, if any, must be small, and perhaps in current determinations of parton distributions (PDFs) are partly absorbed in the form of a distortion of the PDFs themselves.

The aim of this work is to provide a general strategy to quantify potential deviations from NLO DGLAP, and to apply it to existing HERA data. The search for deviations from NLO DGLAP in HERA data has been recently the subject of intense theoretical and experimental activity [8–11]. However, existing studies typically investigate the agreement of the data with predictions of specific models, rather than trying to provide a comparative assessment of the predictions of the models in comparison to NLO DGLAP. Also, the issue of possible dependence of results on the choice of PDFs is usually not addressed. Our approach is meant to provide a model independent assessment of effects beyond NLO DGLAP.

The basic idea of this study is that if deviations from NLO DGLAP in the data are hidden in a distortion of parton distributions, they could be singled out by determining undistorted PDF from data in regions where such effects are small [12]. We will do this in the following way: we determine PDFs using data at large  $x$  and  $Q^2$ , where NLO DGLAP is likely to hold with high accuracy. We then use NLO DGLAP to evolve these PDFs down to the low  $x$  and  $Q^2$  region where deviations are expected to arise, and we compare our predictions to the data in this region, which were not used in the PDF determination. We then search for systematic deviations between data and theory using a variety of statistical tools.

Possible deviations from fixed-order DGLAP could affect phenomenology in two different ways. First, if they were indeed hidden by a distortion of PDFs then this distortion could contaminate LHC observables, which would thus be affected by a hitherto neglected

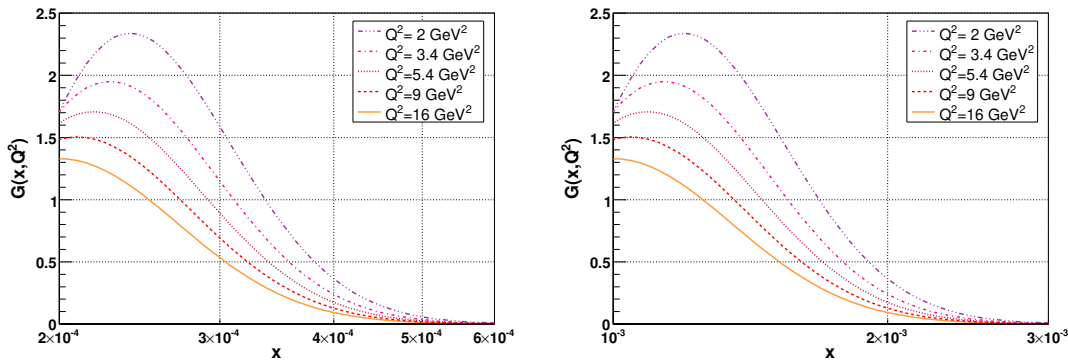


Figure 1: DGLAP backward evolution of a gaussian boundary condition  $G(x, Q_0^2 = 16 \text{ GeV}^2)$  centered at  $\bar{x} = 2 \cdot 10^{-4}$  (left) and  $\bar{x} = 10^{-3}$  (right).

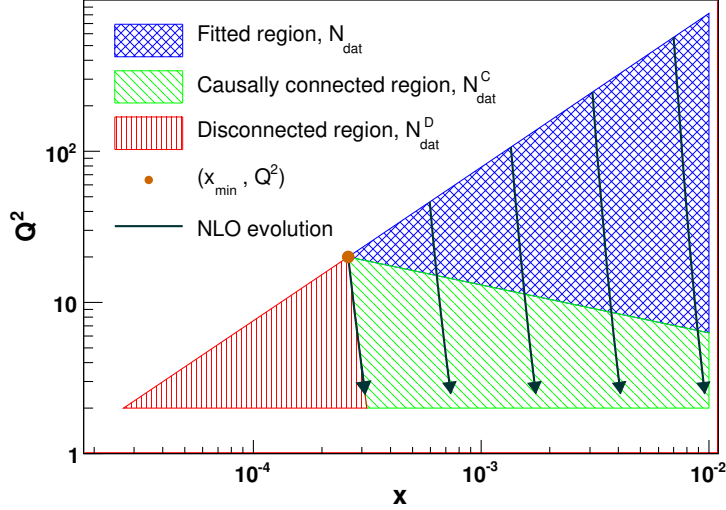


Figure 2: Causal structure of DGLAP evolution in the  $(x, Q^2)$  plane. The arrow lines denote the trajectories followed by the maxima of the curves in Fig. 1. The upper right (blue) region contains the data used to determine PDFs which are then evolved to the causally connected (green) region below it. No information can be obtained on the (red) 'disconnected' region in the lower left corner. In practice, the boundary between the connected and disconnected region will be approximated by a vertical line with  $x = x_{\min}$ . The number of data points in each region are listed in Table 1 below.

uncertainty. We will address this issue, which has already been raised in the past with somewhat contradictory conclusions [13, 14] in the last part of this paper. Second, such deviations might provide evidence for effects which, if included systematically, could affect LHC observables in a non-negligible way. For instance, recent computation of small  $x$  resummation corrections to various hard processes [15–19] shows that their effect at the LHC is expected to be of the same size or larger than NNLO corrections. Our results may support the need for a systematic inclusion of these effects.

Because our basic strategy consists of comparing to data the results of perturbative evolution, we must first discuss which kinematic regions are connected by perturbative evolution in a causal way, i.e., such that the results of evolution to one region are affected by a change in the boundary condition in the other region. The DGLAP evolution equation for the vector of PDFs  $f(x, Q^2)$  has the form

$$Q^2 \frac{df(x, Q^2)}{dQ^2} = \int_x^1 \frac{dy}{y} P\left(\alpha_s(Q^2), \frac{x}{y}\right) f(y, Q^2) , \quad (1)$$

where  $P(\alpha_s, x)$  is a splitting function matrix. Because of the convolution, the solution  $f(\bar{x}, \bar{Q}^2)$  of Eq. (1) at some point  $z = (\bar{x}, \bar{Q}^2)$  only depends on the boundary condition  $f(y, Q_0^2)$  in the range  $y \in [\bar{x}, 1]$ . Hence, a priori the past causal cone of the point  $(\bar{x}, \bar{Q}^2)$  is given by the region  $(x > \bar{x}, Q^2 < \bar{Q}^2)$ .

However, the bulk of the contribution to the convolution integral Eq. (1) comes from a small range in  $x$ , so that in practice evolution mostly proceeds along trajectories that go along a path from larger  $(x_0, Q_0^2)$  to smaller  $(\bar{x}, \bar{Q}^2)$ . This picture in fact becomes

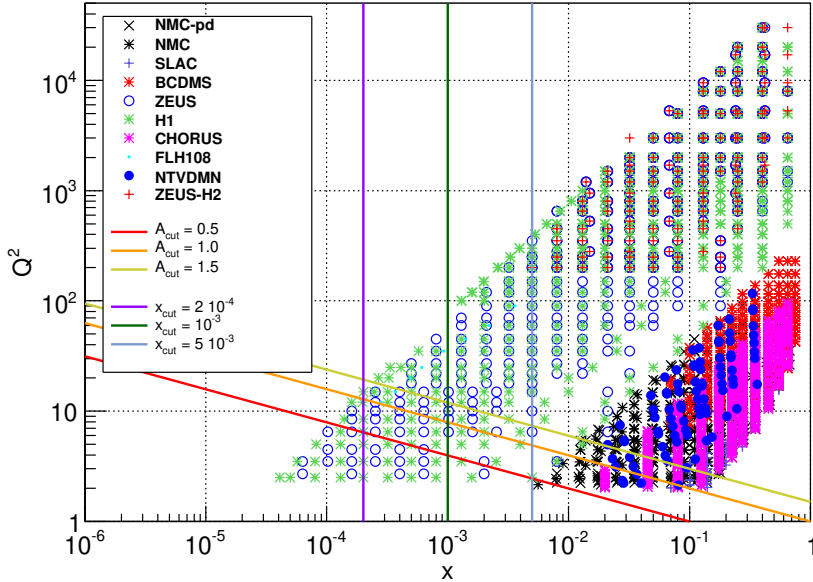


Figure 3: The NNPDF1.2 data set with the various kinematic cuts applied in the present study.

exact in the small  $x$ , large  $Q^2$  limit, in which NLO DGLAP evolution is given by a wave equation which may be studied using the method of characteristics [20, 21]. In Fig. 1 we show the evolution of two gaussian boundary conditions centered around different  $\bar{x}$  from  $Q_{\text{in}}^2 = 16 \text{ GeV}^2$  down to  $Q_{\text{fin}}^2 = 2 \text{ GeV}^2$ , obtained solving the NLO DGLAP equation numerically with the HOPPET [22] package. Clearly, for the reasonably short evolution lengths shown, similar to those which we shall consider in the sequel, the peaks remain localized enough, and traverse approximately linear trajectories. These trajectories are drawn as arrow lines in Fig. 2, and turn out to be almost parallel to the  $y$ -axis, consistent with the intuition that DGLAP evolution is evolution in  $Q^2$  at almost fixed  $x$ . In conclusion, if we know parton distributions for  $x > \bar{x}$  at some scale  $Q_0^2$  then DGLAP evolution allows us to determine them for all  $x > x_{\text{min}}$  at any other scale  $Q^2$ . However, for the evolution lengths displayed in Fig. 1,  $x_{\text{min}} \approx \bar{x}$  to an accuracy of a few percent.

We conclude that we can gain information on the low  $x$ , low  $Q^2$  region (where we expect possible deviations from NLO DGLAP) provided only we have data at larger  $Q^2$  in the same low  $x$  region. However, as  $Q^2$  is raised, we expect deviations to only arise at increasingly smaller  $x$ . Indeed, we tentatively expect deviations to appear when  $Q^2 < Q_{\text{cut}}^2(x)$ , with

$$Q_{\text{cut}}^2(x) \equiv A_{\text{cut}} x^{-\lambda}, \quad (2)$$

where  $\lambda \approx 0.3$ . This choice corresponds to the kinematic region where the so-called geometric scaling [23] of structure function data can no longer be understood as a consequence of fixed-order DGLAP [24] and could thus be evidence for effects beyond DGLAP. We will thus fit data with  $Q^2 > Q_{\text{cut}}^2(x)$  in order to gain information on the low  $Q^2$  region which is causally connected to it. These regions are shown (for the choice  $A_{\text{cut}} = 1.5$ ) in Fig. 2.

We have thus performed a PDF determination based on the methodology and dataset

| $A_{\text{cut}}$ | $N_{\text{dat}}$ | $N_{\text{dat}}^C$ | $N_{\text{dat}}^D$ | $(x_{\text{min}}, Q^2 [\text{GeV}^2])$ |
|------------------|------------------|--------------------|--------------------|--|
| no cuts          | 3372             | 0                  | 0                  | $(4.1 \cdot 10^{-5}, 2.5)$             |
| 0.2              | 3363             | 4                  | 5                  | $(8 \cdot 10^{-5}, 3.5)$               |
| 0.3              | 3350             | 14                 | 8                  | $(10^{-4}, 6.5)$                       |
| 0.5              | 3333             | 25                 | 15                 | $(1.4 \cdot 10^{-4}, 8.5)$             |
| 0.7              | 3304             | 38                 | 16                 | $(1.6 \cdot 10^{-4}, 12)$              |
| 1.0              | 3228             | 44                 | 19                 | $(2.1 \cdot 10^{-4}, 15)$              |
| 1.2              | 3164             | 53                 | 30                 | $(2.4 \cdot 10^{-4}, 15)$              |
| 1.5              | 3084             | 59                 | 38                 | $(2.7 \cdot 10^{-4}, 20)$              |

Table 1: Number of data points from Fig. 3 in the regions of the  $(x, Q^2)$  plane defined according to Fig. 2 with the cut Eq. (2). The columns show, from left to right: the value of  $A_{\text{cut}}$  Eq. (2) used in the cut; the total number of points  $N_{\text{dat}}$  which pass the cut; the number of points  $N_{\text{dat}}^C$  in the causally connected region; the number of points  $N_{\text{dat}}^D$  in the disconnected region; the minimum value of  $(x_{\text{min}}, Q^2)$  for the data region (coordinates of the point denoted by a dark (brown) dot in Fig. 2). The total number of points  $N_{\text{dat}}$  refers to all experiments shown in Fig. 3, while the number of points in the connected and disconnected regions refer to HERA data only (not including  $F_L$  data).

of the NNPDF1.2 parton set [7], but only including data which pass the cut  $Q^2 > Q_{\text{cut}}^2(x)$  Eq. (2) with various choices of  $A_{\text{cut}}$  and  $\lambda = 0.3$ . The data and various cuts are displayed in Fig. 3; the number of points in the fitted, causally connected, and disconnected regions (defined as in Fig. 2) are listed in Table 1. The fitted data include essentially all available inclusive deep-inelastic scattering (DIS) data, as well as neutrino dimuon data, which are necessary in order to constrain the strange PDF. The numbers given in Table 1 for the data in the causally connected and disconnected regions refer only to HERA data (not including  $F_L$ ), which will be used in the analysis below.

The NNPDF methodology [25, 26] is especially suited to this analysis because it provides a determination of PDFs and their uncertainty which is independent of the choice of data set, and which has been shown in benchmark studies [27] to behave in a statistically consistent way when data are added or removed to the fit. Also, because of the use of a Monte Carlo approach, the NNPDF methodology is easily amenable to the use of standard statistical analysis tools as we shall see below. This methodology has been applied successfully to determination of parton distributions [7, 25, 26, 28, 29], unpolarized [30, 31] and polarized [32] structure functions, QCD spectral functions [33] and atmospheric neutrino fluxes [34].

The main drawback of current NNPDF parton fits is the way heavy quarks are treated, namely, the fact the so-called zero-mass variable-flavour number scheme is used. This means that terms which are suppressed by powers of heavy quark mass over the large scale of the process are neglected, which is a poor approximation close to the threshold for heavy quark production. This may be a problem for our analysis because most of the data we are interested in is close to the charm threshold. This issue will have to be addressed when analyzing our results.

The results of our fits with various cuts are compared to the standard NNPDF1.2 fit and to experimental data in Fig. 4. We show the structure function  $F_2(x, Q^2)$  in the small  $x$  region, both at a scale in the data region (left) and at a low scale in the region which

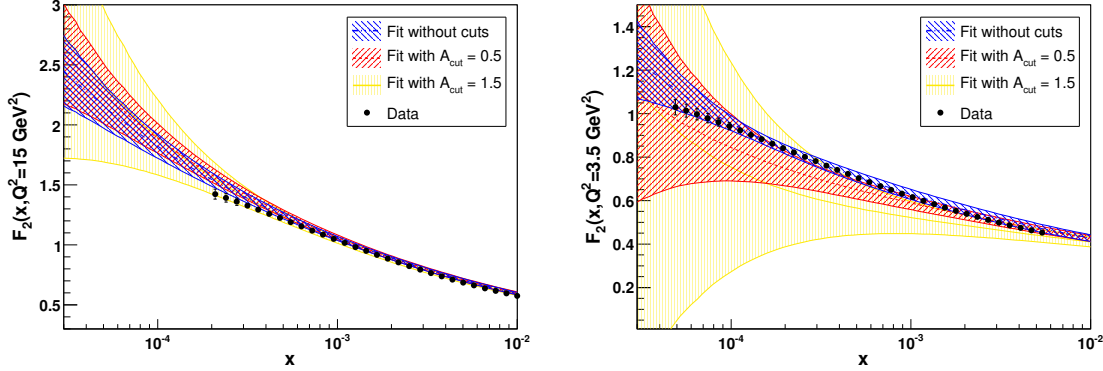


Figure 4: The proton structure function  $F_2(x, Q^2)$  at small  $x$ , computed from PDFs obtained from fits with different values of  $A_{\text{cut}}$ , for  $Q^2 = 15 \text{ GeV}^2$  (left) and  $Q^2 = 3.5 \text{ GeV}^2$  (right), compared to the data. Wider uncertainty bands correspond to more restrictive cuts.

is causally connected to it (right), with no cut (standard NNPDF1.2 fit [7]) and with the lowest and highest of the cuts of Fig. 3. Instead of showing directly the data used in the fit, we display the very precise interpolation of the data of Ref. [31], which is more accurate than any individual data point because it combines all data in a way which does not depend on theory or model assumptions.

It is clear that at the high scale  $Q^2 = 15 \text{ GeV}^2$  there is no significant difference in the data region between the three different predictions from the fit without cuts, the one with intermediate cut and the one with the maximum cut. The only difference is the growth of the PDF uncertainty in the extrapolation region, which is statistically expected due to the missing experimental information removed by the cuts. However, at low  $Q^2 = 3.5 \text{ GeV}^2$ , besides showing an increase of uncertainty, the prediction obtained by backward evolution of the data above the cut exhibits a systematic downwards trend: it always lies below the HERA data. As we increase the value of  $A_{\text{cut}}$ , this trend becomes more and more evident, and it turns on smoothly as we move from  $Q^2 = 15 \text{ GeV}^2$  to  $Q^2 = 3.5 \text{ GeV}^2$ . This is to be contrasted to the uncut NNPDF1.2 fit, which always sits on top of the data. It would thus seem that the backward NLO DGLAP evolution of the high-scale data is too strong: it overestimates the actual amount of evolution seen in the data themselves.

Before trying to assess more quantitatively the size of this effect, let us first examine how the cuts affect the individual PDFs. In Fig. 5 we show the singlet and the gluon PDFs, which are largest at small  $x$ , for the uncut fit and for two different kinematical cuts. We observe that the cut produces both a sizable increase in PDF uncertainties, especially at small  $x$ , and a change in central values which seems to follow a systematic trend as the cut is moved. However, all PDFs are consistent with each other at the one sigma level, which implies that predictions for physical observables obtained from any of these PDFs will also be compatible at this level, as we shall see explicitly below.

A quantitative estimate of possible deviations can be obtained by defining the statistical distance between a data point  $F_{\text{data},i}$  with uncertainty  $\sigma_{\text{data},i}$  and the associated

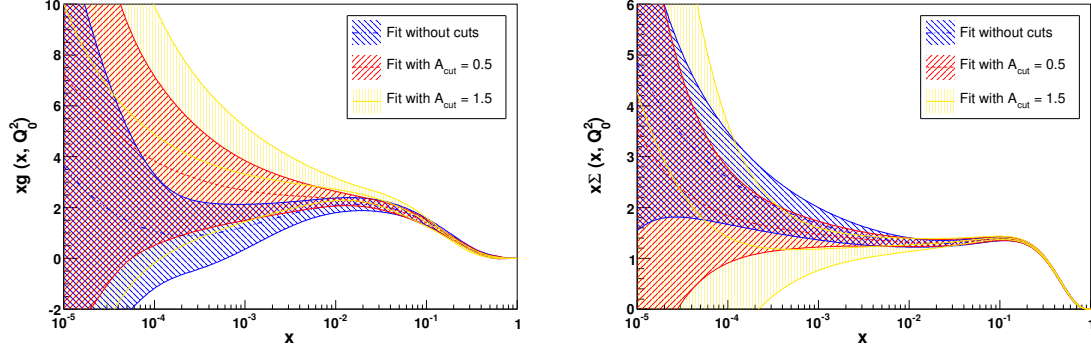


Figure 5: Gluon and singlet PDFs with different cuts at the scale  $Q_0^2 = 2 \text{ GeV}^2$ .

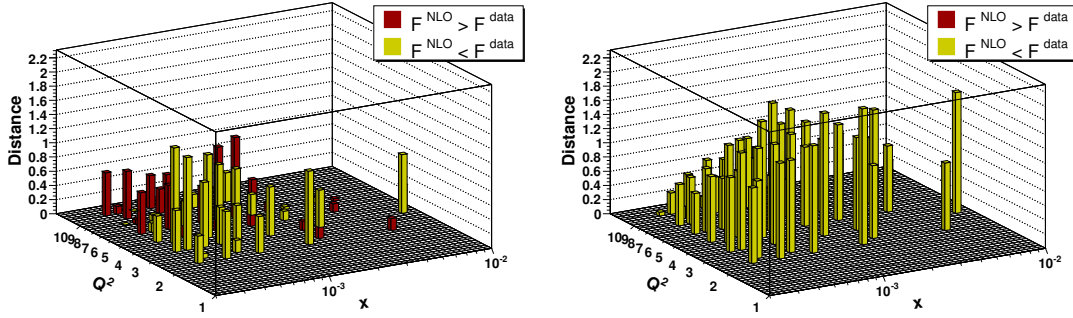


Figure 6: Statistical distance, Eq. (3), between the data in the region excluded from the fit but causally connected to it, and the prediction obtained using NLO DGLAP evolution of the data included in the fit, with  $A_{\text{cut}} = 1.5$ . The distance is computed both when the cut is not applied (left) and when it is applied (right). Dark (red) bars denote negative distances (fit above the data) while light (yellow) bars denote positive distances (data above the fit). The average values of these distances are listed in Table 2.

theoretical prediction  $F_{\text{th},i}$  with uncertainty  $\sigma_{\text{th},i}$

$$d_i^{\text{stat}} \equiv \frac{F_{\text{data},i} - F_{\text{th},i}}{\sqrt{\sigma_{\text{data},i}^2 + \sigma_{\text{th},i}^2}}. \quad (3)$$

where  $\sigma_{\text{th},i}$  stands for the PDF uncertainty. In order to determine the absolute scale of these deviations from NLO DGLAP, we also define the relative distance

$$d_i^{\text{rel}} \equiv \frac{F_{\text{data},i} - F_{\text{th},i}}{(F_{\text{data},i} + F_{\text{th},i})/2}. \quad (4)$$

Whereas  $d_i^{\text{stat}}$  measures the statistical significance of the deviation,  $d_i^{\text{rel}}$  measures its absolute size.

In Fig. 6 (right plot) we show the statistical distance Eq. (3) between the prediction obtained from backward NLO DGLAP evolution of the fit to data above the cut to its causally connected region, and data in this region, for the  $A_{\text{cut}} = 1.5$  case. As a control

| $A_{\text{cut}}$ for the fit | $\langle d^{\text{stat}} \rangle$ |                              |                              |                        |
|------------------------------|-----------------------------------|------------------------------|------------------------------|------------------------|
|                              | $A_{\text{cut}} < 0.5$            | $0.5 < A_{\text{cut}} < 1.0$ | $1.0 < A_{\text{cut}} < 1.5$ | $A_{\text{cut}} < 1.5$ |
| no cuts                      | $0.6 \pm 0.5$                     | $-0.1 \pm 0.5$               | $-0.1 \pm 0.3$               | $0.06 \pm 0.6$         |
| 0.5                          | $1.4 \pm 0.4$                     | —                            | —                            | $1.4 \pm 0.4$          |
| 1.0                          | $1.2 \pm 0.2$                     | $0.7 \pm 0.3$                | —                            | $0.9 \pm 0.4$          |
| 1.5                          | $1.4 \pm 0.3$                     | $0.9 \pm 0.4$                | $0.6 \pm 0.4$                | $1.0 \pm 0.5$          |

Table 2: Average statistical distance, Eq. (3), between the data in the region excluded from the fit but causally connected to it, and the prediction obtained using NLO DGLAP evolution of the data included in the fit. Each row corresponds to a different cut and thus a different set of data; the case  $A_{\text{cut}} = 1.5$  correspond to the distances shown Fig. 6. Each column gives the average over the subset of data in the pertinent row which would also pass various less restrictive cuts, i.e. from left to right data in regions which are increasingly close to the cut corresponding to the given row. In each case, the average and standard deviation of the distance for all points included in the corresponding region. All HERA data (not including  $F_L$  data) shown in Fig. 3 are used; total numbers of data points for each cut are listed in Tab. 1.

| $A_{\text{cut}}$ for the fit | $\langle d^{\text{rel}} \rangle$ |                              |                              |                          |
|------------------------------|----------------------------------|------------------------------|------------------------------|--------------------------|
|                              | $A_{\text{cut}} < 0.5$           | $0.5 < A_{\text{cut}} < 1.0$ | $1.0 < A_{\text{cut}} < 1.5$ | $< A_{\text{cut}} < 1.5$ |
| no cuts                      | $0.03 \pm 0.03$                  | $-0.004 \pm 0.02$            | $-0.006 \pm 0.01$            | $0.01 \pm 0.03$          |
| 0.5                          | $0.13 \pm 0.05$                  | —                            | —                            | $0.13 \pm 0.05$          |
| 1.0                          | $0.22 \pm 0.06$                  | $0.06 \pm 0.03$              | —                            | $0.13 \pm 0.09$          |
| 1.5                          | $0.27 \pm 0.07$                  | $0.08 \pm 0.03$              | $0.03 \pm 0.02$              | $0.12 \pm 0.11$          |

Table 3: Same as Table 2 but for the relative distance Eq. (4).

sample, we also compute and show (left plot) the distance when the data in the cut region are not excluded from the fit. Distances are computed using HERA data only (not including  $F_L$  data) because of their greater consistency (non-HERA data in these regions are extremely scarce anyway). Comparing the two plots, it is clear that when all data are included in the fit the sign of the distances are distributed randomly (the fit is equally likely to be above or below the data), and typically  $d^{\text{stat}} \lesssim 1$ . However, when the data are excluded from the plot, the fit tends to systematically undershoot the data (almost all distances are positive), while their size is systematically somewhat larger,  $d^{\text{stat}} \gtrsim 1$ . Also, the size of the distance tends to increase somewhat if the data are further away from the cut.

The same conclusion is obtained by inspecting the values of the distance, which are tabulated in Table 2 with various cuts, and in the various regions which are excluded by them. Namely, if no cut is applied, the distances are small and fluctuate randomly. Once a cut is applied, the distances become all positive, and they show a tendency to increase when the data are further away from the cut. This confirms the qualitative features seen in Fig. 6: there is evidence for a statistically significant deviation of the data from the NLO DGLAP prediction. The evidence is only at the one-sigma level, but it is systematic, and its significance tends to increase when the amount of evolution required to get to the given point or region is larger, despite the fact that points with longer evolution lengths are those at the lowest  $x$  and  $Q^2$  and thus affected by the largest uncertainties.

We can study the absolute size of the effect by repeating the same analysis, but now for



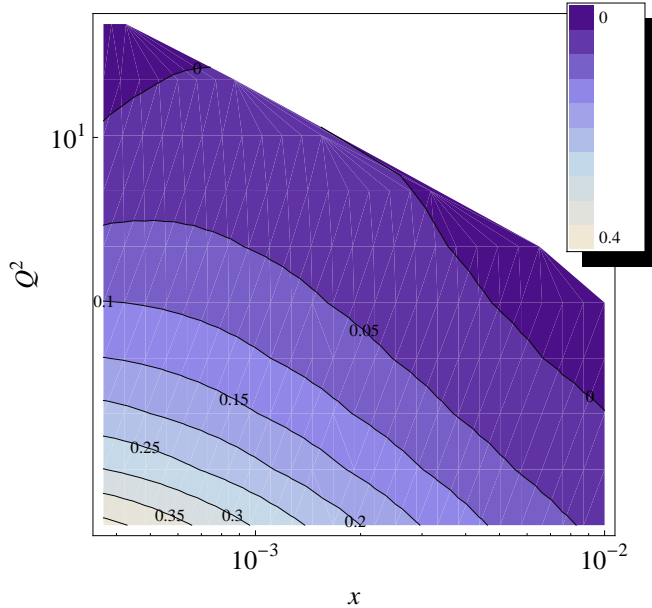


Figure 7: Contour plot of the relative distances. Eq. (4), with the most restrictive cut  $A_{\text{cut}} = 1.5$ . Distances are computed between the NLO DGLAP and the parametrization of the data Ref. [31].

the relative distance Eq. (4). Results are collected in Table 3: it is clear that the deviation increases in size as the region of the comparison is further away from the fitted region, as one would expect of a deviation driven by the evolution length. A contour plot of the distances, Fig. 7, clearly shows the increase of the distance with the evolution length.

The behaviour of the statistical and relative distances as a function of  $A_{\text{cut}}$  is summarized in Fig. 8, where we show the distances in the first column of Tables 2-3, including also the further intermediate values of  $A_{\text{cut}}$  shown in Table 1. These values correspond in each case to the data in the causally connected region which are further away from the cut. The increase of the relative distance (right), and the general trend of an increase of its significance (left) can both be seen clearly.

As a final piece of evidence, we also show in Table 4 the the  $\chi^2$  for the points of Table 1 excluded by various cuts, in the causally connected region for each cut, and compare them to the values obtained in the absence of a cut. In each case, the quality of the fit when the data are not fitted is significantly worse, and it gets worse when the cut is more restrictive, i.e. more data require more evolution. Note that both in the NNPDF fits [7, 26] and in benchmarks [27] it has been explicitly checked that when groups of data (in individual regions, or from particular experiments) are removed from the NNPDF fit, the quality of the NNPDF fit to those data does not deteriorate, because uncertainty bands always widen in such a way that the statistical compatibility of the fit with the excluded data is unchanged. Hence, we must conclude that in this specific kinematic region there is a deviation from the fit which is statistically significant and whose origin is not statistical.

We conclude therefore that we have a statistically significant indication that data at low  $x$  and  $Q^2$  deviate from the prediction of NLO DGLAP evolution. One may therefore

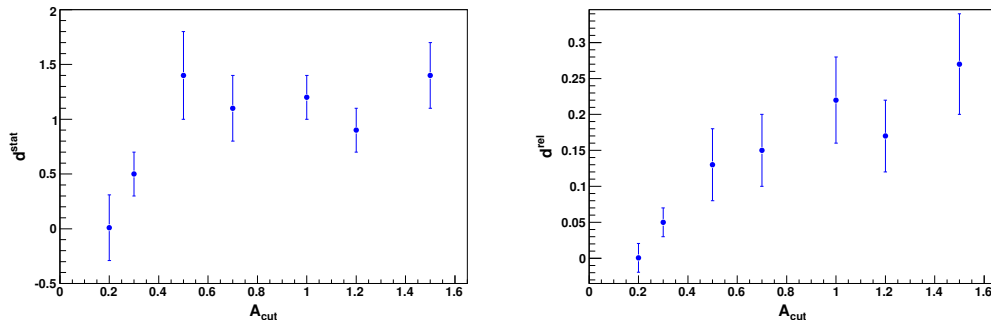


Figure 8: Statistical distances Eq. (3) (left) and relative distances Eq. (4) (right) for fits with different  $A_{\text{cut}}$  as a function of  $A_{\text{cut}}$ , for all the choices of cuts of Table 1. The distances shown are all computed for the subset of points of each fit which also satisfies the cut  $A_{\text{cut}} < 0.5$ , i.e. they correspond to the first column of Tables 2-3.

| $A_{\text{cut}}$ | $\chi^2_{\text{without cuts}}$ | $\chi^2_{\text{with cut}}$ |
|------------------|--------------------------------|----------------------------|
| 0.5              | 19.68/25 = 0.79                | 106.22/25 = 4.25           |
| 1.0              | 54.41/44 = 1.24                | 138.24/44 = 3.14           |
| 1.5              | 62.31/59 = 1.06                | 860.65/59 = 14.6           |

Table 4: The  $\chi^2$  for all the points in the causally connected region, third column in Table 1, when they are excluded by a cut, compared to the  $\chi^2$  for the same points in the fit without cuts.

ask what are the possible sources of these deviations. One source is readily identified, namely, heavy quark mass effects. Indeed, as already mentioned, the zero-mass variable flavour number scheme used by NNPDF is not accurate in the charm threshold region, which largely overlaps with the region under consideration here. These effects go in the same direction as the deviation found here: the charm quark mass suppresses perturbative evolution driven by charm radiation and its mixing with gluons [35]. However, the size of these effects was recently assessed quantitatively in Ref. [36], where it was found that it is never above 15% for  $F_2$ , while we find deviations as large as 35% at the smallest  $x$  and  $Q^2$  values. We conclude that even though heavy quarks could be partly responsible for the effect that we have seen, they are unlikely to be the only explanation.

We therefore look at other possible reasons for deviation from NLO DGLAP predictions. Whereas a detailed quantitative study is beyond the scope of this work, we briefly examine whether some known potential sources of deviations from the NLO DGLAP prediction are qualitatively compatible with our findings. The first and most natural explanation is that the deviation is due to higher order perturbative corrections, specifically NNLO, which are obviously more important at low scale, and are also known to grow at small  $x$ . However, NNLO corrections at small  $x$  are known to lead to a stronger scale dependence of  $F_2(x, Q^2)$  in comparison to the NLO prediction. This can be seen both in global NNLO fits [3, 37] and from a study of anomalous dimensions and  $K$ -factors obtained from them [4, 38]. Therefore, the inclusion of these effects would actually make the discrepancy worse.

However, it is well-known that perturbation theory becomes unstable at small  $x$  and must be resummed. The all-order resummation of small  $x$  corrections to perturbative

| $A_{cut}$ | $\sigma_{W+\mathcal{B}_{l+\nu_l}}$ (nb) | $\sigma_{W-\mathcal{B}_{l-\nu_l}}$ (nb) | $\sigma_{Z\mathcal{B}_{l+l-}}$ (nb) | $\sigma_{gg\rightarrow H}$ (pb) | $\sigma_{t\bar{t}}$ (pb) |
|-----------|---|---|-------------------------------------|---------------------------------|--------------------------|
| no cuts   | $11.93 \pm 0.30$                        | $8.43 \pm 0.20$                         | $1.96 \pm 0.04$                     | $36.6 \pm 1.1$                  | $907 \pm 23$             |
| 0.2       | $11.95 \pm 0.33$                        | $8.46 \pm 0.21$                         | $1.96 \pm 0.04$                     | $36.6 \pm 1.0$                  | $908 \pm 22$             |
| 0.3       | $11.99 \pm 0.41$                        | $8.50 \pm 0.27$                         | $1.97 \pm 0.06$                     | $36.5 \pm 1.0$                  | $904 \pm 28$             |
| 0.5       | $12.23 \pm 0.37$                        | $8.62 \pm 0.23$                         | $2.00 \pm 0.05$                     | $36.8 \pm 0.9$                  | $886 \pm 29$             |
| 0.7       | $12.23 \pm 0.36$                        | $8.68 \pm 0.27$                         | $2.01 \pm 0.05$                     | $37.0 \pm 1.0$                  | $874 \pm 35$             |
| 1.0       | $12.43 \pm 0.46$                        | $8.71 \pm 0.28$                         | $2.02 \pm 0.05$                     | $37.4 \pm 1.1$                  | $865 \pm 34$             |
| 1.2       | $12.23 \pm 0.46$                        | $8.66 \pm 0.28$                         | $2.00 \pm 0.06$                     | $37.6 \pm 1.9$                  | $875 \pm 35$             |
| 1.5       | $12.45 \pm 0.44$                        | $8.72 \pm 0.25$                         | $2.03 \pm 0.05$                     | $37.7 \pm 1.2$                  | $858 \pm 36$             |

Table 5: Results for LHC observables computed with PDFs obtained from fits to reduced datasets based on the ‘ $A_{cut}$ ’ kinematic cuts Eq. (2).

evolution, properly matched to fixed-order DGLAP evolution [4], in the HERA region leads to an effect that is qualitatively opposite to that of NNLO corrections, namely to a weaker scale dependence in comparison to NLO, as one can again see from a study of anomalous dimensions and  $K$ -factors obtained from them [4, 27, 38]. It follows that small  $x$  resummation could explain the deviation that we observe.

Perturbative evolution at small  $x$  is expected to eventually be corrected by non-linear terms, related to high parton densities, which should restore unitarity in the very high energy limit [5]. The precise signature of these effects is not easy to assess, because it is nontrivial to match these effects to DGLAP evolution, hence their predictions are usually given close to the asymptotic high-energy limit, while their scale dependence is not easily determined. However, the leading nonlinear corrections to perturbative evolution, first studied in Ref. [39], correspond to a suppression of perturbative evolution due to gluon recombination. Therefore, to the extent that saturation dynamics reproduces this suppression, we expect it to be roughly compatible with the effect we observe.

Let us finally turn to the possible impact of the deviations we found on LHC phenomenology. Indeed, if NLO DGLAP is affected by corrections in the small  $x$ , small  $Q^2$  part of the kinematic region which is currently used for parton determination, one must conclude that current parton sets, which use DGLAP evolution throughout, will be affected by some bias due to lack of proper inclusion of the necessary corrections to DGLAP evolution. We will now assess the size of this bias, and its impact on LHC observables.

In order to do this, we compute LHC observables using the PDFs obtained with a variety of kinematic cuts: the PDFs obtained with more restrictive cuts will be bias-free, while those obtained without cuts might be biased. The difference between the observables computed in these cases will thus give an indication of the possible amount of bias. On top of the cuts of the form Eq. (2) that we discussed so far we will now also consider the impact on PDF extraction of  $Q^2$ -independent cuts in  $x$  of the form

$$x_i \geq x_{cut}. \quad (5)$$

These cuts have been considered previously [13, 14]; we will take the same values of  $x_{cut}$  as in these references. In comparison to the cuts Eq. (2) one would expect them to be equally effective in removing effects beyond NLO DGLAP, but to also remove small  $x$  data at larger  $Q^2$ , with consequent loss of accuracy.

|              | $\sigma_{W^+\mathcal{B}_{l+\nu_l}}$ (nb) | $\sigma_{W^-\mathcal{B}_{l-\nu_l}}$ (nb) | $\sigma_Z\mathcal{B}_{l+l^-}$ (nb) | $\sigma_{gg\rightarrow H}$ (pb) | $\sigma_{t\bar{t}}$ (pb) |
|--------------|--|--|------------------------------------|---------------------------------|--------------------------|
| no cuts      | $11.93 \pm 0.30$                         | $8.43 \pm 0.20$                          | $1.96 \pm 0.04$                    | $36.6 \pm 1.1$                  | $907 \pm 23$             |
| $x > 0.0002$ | $11.90 \pm 0.32$                         | $8.39 \pm 0.23$                          | $1.95 \pm 0.04$                    | $36.5 \pm 1.0$                  | $909 \pm 24$             |
| $x > 0.001$  | $12.11 \pm 0.36$                         | $8.55 \pm 0.19$                          | $1.98 \pm 0.04$                    | $37.0 \pm 0.9$                  | $894 \pm 25$             |
| $x > 0.0025$ | $12.75 \pm 1.39$                         | $8.78 \pm 0.62$                          | $2.05 \pm 0.15$                    | $37.0 \pm 1.1$                  | $886 \pm 45$             |
| $x > 0.005$  | $12.46 \pm 1.72$                         | $8.74 \pm 0.93$                          | $2.03 \pm 0.22$                    | $36.7 \pm 0.9$                  | $877 \pm 51$             |

Table 6: Results for LHC observables computed with PDFs obtained from fits to reduced datasets based on the ‘ $x_{\text{cut}}$ ’ kinematic cuts Eq. (5).

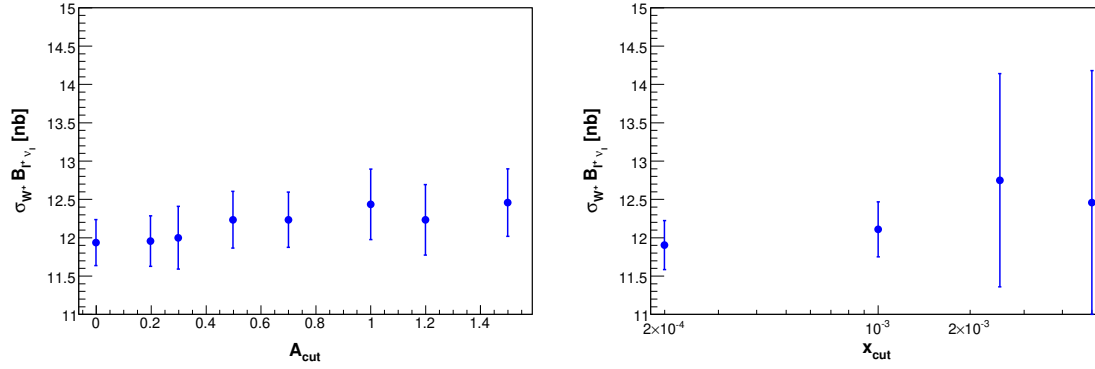


Figure 9:  $W^+$  cross section for different cuts. Left: ‘ $A_{\text{cut}}$ ’-based fits. Right: ‘ $x_{\text{cut}}$ ’-based fits.

Using the PDFs obtained in all these ways, we have computed the  $W^\pm$ ,  $Z^0$ ,  $t\bar{t}$  and  $gg \rightarrow H$  total NLO cross sections for LHC kinematics (at 14 TeV) using the MCFM code [40]. Results are summarized in Tables 5 and 6 and in a graphical way in Figs. 9 and 10. Clearly, central values for all observables with the exception of Higgs production change significantly as the cut is raised. However, PDF uncertainties increase accordingly, in such a way that the observables from the fits from reduced datasets remain always compatible with the observables from the reference fit. The greater stability of the Higgs production cross section can be understood as a consequence of the fact that it depends essentially on the large- $x$  gluon, which is essentially unaffected by the cuts, while the other observables depend also on the small  $x$  behaviour of PDFs. Interestingly, as the cut is raised the shift in central values of observables (such as  $W$  and  $Z$  production) is similar to that induced by the inclusion of charm mass effects [6, 36], consistent with our observation that these effects could explain part of the discrepancy with NLO DGLAP that we find.

If we compare ‘ $A_{\text{cut}}$ ’ fits (based on cuts Eq. (2)) and ‘ $x_{\text{cut}}$ ’ fits (based on cuts Eq. (5)), we see that there the loss of accuracy in the latter case is considerably larger. Therefore, an optimal choice of ‘conservative’ [13] partons, which minimizes the impact of possible non-standard effects while maximizing the use of available information, could be based on the choice of a cut of the form Eq. (2). Also, due to this large increase in the PDF uncertainty, we do not have evidence of inconsistencies between PDFs obtained from ‘ $x_{\text{cut}}$ ’ fits and the reference, in partial disagreement with the conclusion of Ref. [13], though perhaps this conclusion might also change if one used the more flexible parton parametrization and dynamical tolerance methods recently introduced by the MSTW collaboration [3].

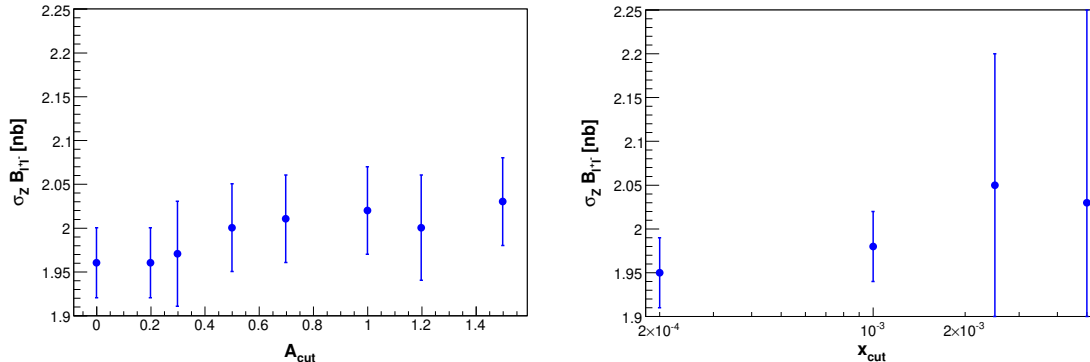


Figure 10:  $Z$  cross section for different cuts. Left: ' $A_{\text{cut}}$ '-based fits. Right: ' $x_{\text{cut}}$ '-based fits.

Our general conclusion is that the possible distortion of NLO PDF sets induced by deviations from NLO DGLAP in the small  $x$  and  $Q^2$  region of the HERA data has an effect on the NLO determination of inclusive LHC observables which is at the percent level. However, the full impact on LHC observables of the dynamics which might cause the deviations (such as small  $x$  resummation) could only be assessed by a dedicated study which goes beyond the scope of this work.

In summary, we have implemented a strategy to single out deviations from fixed order DGLAP evolution in a QCD analysis of inclusive experimental data. We have applied this strategy to a PDF analysis based on the NNPDF framework, and studied the effects of various kinematical cuts in HERA data. The use of several statistical indicators shows clear evidence for deviations between the scale dependence observed in the data and that predicted by NLO DGLAP evolution in the small  $x$  and  $Q^2$  region. Whereas part of these deviations could be removed by a more refined treatment of the charm threshold, the effect is likely to be due to either the resummation of small  $x$  perturbative corrections, or power-suppressed corrections to perturbative evolution. It cannot be explained by invoking NNLO terms, which go in the wrong direction and would make the discrepancy worse. We then have shown that even if these effects induce a distortion of available PDF set, the impact of this distortion on the NLO computation of standard candle LHC observables is small in comparison to current PDF uncertainties. It might however become more significant in future precision studies, especially if deep-inelastic scattering data at higher energy were available, such as those which might be obtained at a future electron-hadron collider based on the LHC (LHeC) [41, 42]. More interestingly, if the cause of these effects were established with certainty, it might require a nontrivial reassessment of the determination of LHC observables: for example, by a systematic inclusion of small  $x$  resummation effects.

### Acknowledgements

We thank all the members of the NNPDF collaboration, which has developed the PDF fitting methodology and code on which this study is based. We acknowledge discussions with J. L. Albacete, N. Armesto and G. Milhano. This work was partly supported by the European network HEPTOOLS under contract MRTN-CT-2006-035505.

## References

- [1] G. Altarelli and G. Parisi, Nucl. Phys. B **126**, 298 (1977).  
V. N. Gribov and L. N. Lipatov, Sov. J. Nucl. Phys. **15**, 438 (1972) [Yad. Fiz. **15**, 781 (1972)].  
Y. L. Dokshitzer, Sov. Phys. JETP **46**, 641 (1977) [Zh. Eksp. Teor. Fiz. **73**, 1216 (1977)].
- [2] S. Moch, J. A. M. Vermaseren and A. Vogt, Nucl. Phys. B **688** (2004) 101 [arXiv:hep-ph/0403192].  
A. Vogt, S. Moch and J. A. M. Vermaseren, Nucl. Phys. B **691** (2004) 129 [arXiv:hep-ph/0404111].  
J. A. M. Vermaseren, A. Vogt and S. Moch, Nucl. Phys. B **724** (2005) 3 [arXiv:hep-ph/0504242].
- [3] A. D. Martin, W. J. Stirling, R. S. Thorne and G. Watt, Eur. Phys. J. C **63** (2009) 189 [arXiv:0901.0002 [hep-ph]].
- [4] G. Altarelli, R. D. Ball and S. Forte, Nucl. Phys. B **799** (2008) 199 [arXiv:0802.0032 [hep-ph]],  
M. Ciafaloni, D. Colferai, G. P. Salam and A. M. Stasto, JHEP **0708** (2007) 046 [arXiv:0707.1453 [hep-ph]],  
M. Dittmar *et al.*, arXiv:hep-ph/0511119,  
and references therein.  
See also C. D. White and R. S. Thorne, Phys. Rev. D **75** (2007) 034005 [arXiv:hep-ph/0611204].
- [5] "Parton saturation and geometric scaling", in M. Dittmar *et al.*, arXiv:0901.2504 [hep-ph],  
E. Iancu and R. Venugopalan, arXiv:hep-ph/0303204,  
K. Golec-Biernat, arXiv:0812.1523 [hep-ph],  
and references therein.
- [6] P. M. Nadolsky *et al.*, Phys. Rev. D **78** (2008) 013004 [arXiv:0802.0007 [hep-ph]].
- [7] R. D. Ball *et al.* [The NNPDF Collaboration], Nucl. Phys. B **823** (2009) 195 [arXiv:0906.1958 [hep-ph]].
- [8] J. Ellis, H. Kowalski and D. A. Ross, Phys. Lett. B **668** (2008) 51 [arXiv:0803.0258 [hep-ph]].
- [9] E. Iancu, K. Itakura and S. Munier, Phys. Lett. B **590** (2004) 199 [arXiv:hep-ph/0310338].
- [10] J. L. Albacete, N. Armesto, J. G. Milhano and C. A. Salgado, Phys. Rev. D **80** (2009) 034031 [arXiv:0902.1112 [hep-ph]].

- [11] H. Weigert, Prog. Part. Nucl. Phys. **55** (2005) 461 [arXiv:hep-ph/0501087].
- [12] F. Gélis, talk at HERALHC, CERN, May 2008;  
[http://indico.cern.ch/getFile.py/  
access?contribId=4&sessionId=0&resId=0&materialId=slides&confId=27458](http://indico.cern.ch/getFile.py/access?contribId=4&sessionId=0&resId=0&materialId=slides&confId=27458)
- [13] A. D. Martin, R. G. Roberts, W. J. Stirling and R. S. Thorne, Eur. Phys. J. C **35**, 325 (2004) [arXiv:hep-ph/0308087].
- [14] J. Huston, J. Pumplin, D. Stump and W. K. Tung, JHEP **0506** (2005) 080 [arXiv:hep-ph/0502080].
- [15] R. D. Ball and R. K. Ellis, JHEP **0105** (2001) 053 [arXiv:hep-ph/0101199].
- [16] R. D. Ball, Nucl. Phys. B **796** (2008) 137 [arXiv:0708.1277 [hep-ph]].
- [17] S. Marzani, R. D. Ball, V. Del Duca, S. Forte and A. Vicini, Nucl. Phys. B **800** (2008) 127 [arXiv:0801.2544 [hep-ph]].
- [18] S. Marzani and R. D. Ball, Nucl. Phys. B **814** (2009) 246 [arXiv:0812.3602 [hep-ph]].
- [19] G. Diana, Nucl. Phys. B **824** (2010) 154 [arXiv:0906.4159 [hep-ph]].
- [20] R. D. Ball and S. Forte, Phys. Lett. B **335** (1994) 77 [arXiv:hep-ph/9405320].
- [21] S. Forte and R. D. Ball, Acta Phys. Polon. B **26** (1995) 2097 [arXiv:hep-ph/9512208].
- [22] G. P. Salam and J. Rojo, Comput. Phys. Commun. **180** (2009) 120 [arXiv:0804.3755 [hep-ph]].
- [23] A. M. Stasto, K. J. Golec-Biernat and J. Kwiecinski, Phys. Rev. Lett. **86** (2001) 596 [arXiv:hep-ph/0007192].
- [24] F. Caola and S. Forte, Phys. Rev. Lett. **101** (2008) 022001 [arXiv:0802.1878 [hep-ph]].
- [25] L. Del Debbio, S. Forte, J. I. Latorre, A. Piccione and J. Rojo [NNPDF Collaboration], JHEP **0703** (2007) 039 [arXiv:hep-ph/0701127].
- [26] R. D. Ball *et al.* [NNPDF Collaboration], Nucl. Phys. B **809** (2009) 1 [Erratum-ibid. B **816** (2009) 293] [arXiv:0808.1231 [hep-ph]].
- [27] M. Dittmar *et al.*, arXiv:0901.2504 [hep-ph],  
H. Jung *et al.*, arXiv:0903.3861 [hep-ph].
- [28] J. Rojo *et al.* [NNPDF Collaboration], arXiv:0811.2288 [hep-ph].
- [29] A. Guffanti, J. Rojo and M. Ubiali, arXiv:0907.4614 [hep-ph].
- [30] S. Forte, L. Garrido, J. I. Latorre and A. Piccione, JHEP **0205**, 062 (2002) [arXiv:hep-ph/0204232].
- [31] L. Del Debbio, S. Forte, J. I. Latorre, A. Piccione and J. Rojo [NNPDF Collaboration], JHEP **0503** (2005) 080 [arXiv:hep-ph/0501067].

- [32] L. Del Debbio, A. Guffanti and A. Piccione, arXiv:0907.2506 [hep-ph].
- [33] J. Rojo and J. I. Latorre, JHEP **0401**, 055 (2004) [arXiv:hep-ph/0401047].
- [34] M. C. Gonzalez-Garcia, M. Maltoni and J. Rojo, JHEP **0610**, 075 (2006) [arXiv:hep-ph/0607324].
- [35] P. M. Nadolsky and W. K. Tung, Phys. Rev. D **79** (2009) 113014 [arXiv:0903.2667 [hep-ph]].
- [36] W. K. Tung, H. L. Lai, A. Belyaev, J. Pumplin, D. Stump and C. P. Yuan, JHEP **0702** (2007) 053 [arXiv:hep-ph/0611254].
- [37] S. I. Alekhin, Phys. Lett. B **519** (2001) 57 [arXiv:hep-ph/0107197].
- [38] J. Rojo, G. Altarelli, R. D. Ball and S. Forte, arXiv:0907.0443 [hep-ph].
- [39] A. H. Mueller and J. w. Qiu, Nucl. Phys. B **268** (1986) 427.
- [40] J. M. Campbell and R. K. Ellis, Phys. Rev. D **60** (1999) 113006 [arXiv:hep-ph/9905386].  
J. M. Campbell and R. K. Ellis, Phys. Rev. D **62** (2000) 114012 [arXiv:hep-ph/0006304].
- [41] J. B. Dainton, M. Klein, P. Newman, E. Perez and F. Willeke, JINST **1** (2006) P10001 [arXiv:hep-ex/0603016].
- [42] J. Rojo and F. Caola, arXiv:0906.2079 [hep-ph].